Ocean Modelling 128 (2018) 1–14

Contents lists available at ScienceDirect

Ocean Modelling

journal homepage: www.elsevier.com/locate/ocemod

Mean circulation of the Mid-Atlantic Bight from a climatological data assimilative model

Julia Levin, John Wilkin*, Naomi Fleming, Javier Zavala-Garay

Department of Marine and Coastal Sciences, Rutgers, The State University of New Jersey New Brunswick, New Jersey, USA

ARTICLE INFO

Keywords:
Dynamic topography
Coastal circulation
Climatology
Mid-Atlantic Bight
Data assimilation
ROMS

ABSTRACT

The along-shelf momentum balance of the Mid-Atlantic Bight (MAB) coastal ocean includes a significant contribution from the along-shelf gradient in sea level. This sea level tilt, of order 10^{-7}, and other features of the mean sea level are not captured well in global mean dynamic topography (MDT) derived from hydrographic observations or satellite altimetry and gravity data, and is poorly represented in global and basin scale dynamical models. This is problematic for applications that would use coastal satellite altimeter data to estimate total water level above datum. We have produced a MDT for the MAB using the Regional Ocean Modeling System (ROMS) with 4-dimensional variational (4D-Var) data assimilation configured to obtain climatological annual and monthly mean results. The observations assimilated were a regional hydrographic climatology of temperature and salinity, and long-term mean velocity from HF-radar, shipboard ADCP, and current-meters. Assimilation adjusts the 3-dimensional ocean state, boundary conditions, and air-sea fluxes to minimize the model-data misfit. The assimilation of mean velocity data is vital to obtaining a realistic circulation result. The MDT exhibits a strong across-shelf sea level slope in geostrophic balance with the southwestward mean flow. The subtle along-shelf tilt is recovered and is relatively uniform throughout the MAB inside the 50 m isobath, but on the southern outer shelf it reverses sign and drives significant across-isobath flow, partially draining the southward mean transport. In the north, across-shelf flow is offshore in the surface and bottom Ekman layers, but largely balanced locally by inflow in the interior depth range.

1. Introduction

In applications of sea surface height observation by satellite altimetry, incomplete or erroneous knowledge of the marine geoid and mean sea surface (MSS) often demands that the long-term multi-decadal mean signal be subtracted from the data and that analysis proceeds working with the sea level anomaly. This, however, also removes the Mean Dynamic Topography (MDT) that arises from the geostrophic balance between sea level pressure gradient and the mean oceanic circulation, and to infer *absolute* dynamic topography above a sea level datum, and *total* geostrophic current (mean plus variability), it becomes necessary to provide an independent estimate of MDT.

Calculations of MDT typically entail a combination of the direct approach (subtracting the MSS from the geoid) with refinements to improve resolution and accuracy by incorporating added gravity, altimetry, hydrography, drifter and other in situ observations (Maximenko et al., 2009; Rio et al., 2011; Rio et al., 2014a). Such MDT products have enabled the widespread use of absolute dynamic topography for the analysis of ocean dynamics and as an input to mesoscale data assimilative ocean prediction systems in the open ocean.

Progress over the past decade in extending the validity of altimeter data to within a few kilometers of the coast by the appropriate application of altimeter radar range corrections and re-tracking of radar waveforms proximate to land (Cipollini et al., 2017; Vignudelli et al., 2011) has opened up to coastal oceanographers the opportunity to exploit the dynamical information content of so-called “coastal altimeter” data. However, in the coastal ocean where steep and variable bathymetry exacerbates uncertainty in the geoid and MSS at short length scales (several tens of kilometers), the need to improve the precision of MDT products is acute.

In our region of interest, the Mid-Atlantic Bight (MAB) of the U.S. east coast (Fig. 1), the CNES-CLS13 MDT (Rio et al., 2014a) (also widely referred to as “AVISO MDT”, produced by CLS Space Oceanography and distributed by AVISO https://aviso.altimetry.fr with support from CNES) captures well the mean sea level associated with circulation in the Slope Sea gyre and the adjacent Gulf Stream (Chassignet and Xu, 2017; Rio et al., 2011), but in shallow water on the continental shelf there are characteristics that oceanographers familiar with the locale

* Corresponding author.
E-mail address: jwilkin@rutgers.edu (J. Wilkin).

https://doi.org/10.1016/j.ocemod.2018.05.003
Received 19 December 2017; Received in revised form 10 April 2018; Accepted 15 May 2018
Available online 17 May 2018
1463-5003/

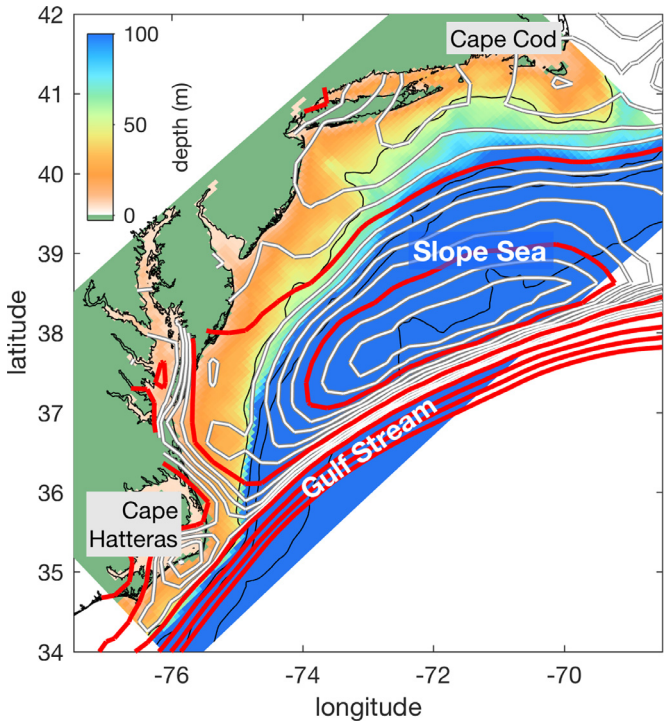

Fig. 1. Mid-Atlantic Bight shelf bathymetry (color shading) in the domain of the ROMS model. Thin black lines additionally show 50, 200, 1000 and 3000 m isobaths. CNES-CLS13 AVISO MDT is shown in red contours at 10 cm intervals highlighting the steep increase southward across the Gulf Stream and white contours at 2 cm intervals selected to show more detail on the MAB shelf. (For interpretation of the references to color in this figure legend, the reader is referred to the web version of this article.)

recognize as unrealistic. These include contours of MDT strongly orthogonal to the coast suggestive of landward geostrophic flow, some closed contours that imply isolated recirculation, and an intense boundary current adjacent to the coast of northern Virginia. In contrast, hydrographic observations, current-meters, drifters and surface currents measured by HF-radar (CODAR) have established that the MAB shelf circulation exhibits a steady shelf-wide southwestward mean along-isobath flow of 5–10 cm s^{-1} (Beardsley and Boicourt, 1981; Gong et al., 2010; Lentz, 2008a; Roarty et al., 2010). Accordingly, regional MDT should show height contours largely parallel to the bathymetry, and a pronounced across-shelf sea level slope. These features are absent from AVISO MDT. Analyses of the MAB momentum balance (Lentz, 2008a; Zhang et al., 2011) have also shown that a subtle along-shelf sea surface tilt of order 10^{-7} (with sea level decreasing toward the south) must be present, which would amount to a 5 cm decrease in sea level from Cape Cod to Cape Hatteras.

It is too much to expect a global product such as AVISO MDT to capture all the subtleties of coastal mean circulation in every shelf sea, but nevertheless these details are vital to using coastal altimeter data in the MAB. Therefore, motivated by the desire to use these data in a regional data assimilative ocean prediction system, we have produced our own local high-resolution MDT for the MAB.

The MAB MDT was computed using the ROMS (Regional Ocean Modeling System) 4-Dimensional Variational (4D-Var) data assimilation (DA) system configured to drive the solution to a steady climatological mean result. The observations assimilated are velocity from HF-radar, long-duration current-meter deployments and shipboard ADCP on an across-shelf transect, and temperature and salinity from a regional hydrographic climatology. The model was forced by climatological mean river inflows and air-sea fluxes, with the DA system adjusting the 3-dimensional (3-D) ocean state, boundary conditions, and air-sea fluxes to minimize the model-data misfit. The analysis was conducted for annual mean and seasonal mean conditions. Following standard practice in satellite altimetry, MDT as we define it does not include the sea level gradient due to atmospheric pressure (the mean Inverted Barometer effect).

Incorporating models in the estimation of regional MDT is not entirely novel. Recognizing that in a DA system MDT error manifests as an observation bias, Dobricic (2005) analyzed statistics from 3 years of simulations from the Mediterranean Forecast System (Pinardi et al., 2003) to iteratively improve a regional MDT. Rio et al., (2014b) improved upon a model-based prior MDT for the Mediterranean Sea by the inclusion of added in situ data, using the model to inform the analysis of the topography of the geopotential reference surface for hydrographic profiles and to suggest correlation length scales for the mapping. In a more geodetic than oceanographic analysis, Mazloff et al., (2014) used altimeter observations and time-varying dynamic topography from a DA model of the California Current to infer stationary errors they ascribed to uncertainties in the geoid at short wavelengths, thereby subsequently decreasing geoid error to obtain a better MDT by the direct method.

The approach we take here differs from these efforts in that we treat MDT as a diagnostic quantity that arises when a high-resolution circulation model enforces dynamical consistency and the influence of coastline and bathymetry on the flow field, with data assimilation further constraining the 3-D flow to match what is known from long term observations.

In addition to providing an MDT for coastal altimetry in our data assimilative ocean forecast system, having a self-consistent 3-D temperature, salinity, velocity and sea level analysis allows us to make inferences about features of the regional mean circulation that go beyond idealized 2-D studies (Lentz, 2008a; Zhang et al., 2011), and also provides a dynamically balanced climatology suited to correcting biases in basin scale model products that we use to set the initial and boundary conditions of our regional forecast model.

The paper is structured as follows. In Section 2 we provide a brief overview of ROMS and its 4D-Var data assimilation system, and follow with descriptions of the ROMS configuration for the MAB, the long-term mean data sets assimilated, and how we implement 4D-Var to compute a solution for the mean circulation. Section 3 presents results from a set of experiments that assimilate successively more comprehensive data sets. Features of the dynamic topography and 3-D ocean circulation are discussed in Section 4, and outcomes are summarized in Section 5.

2. Methods

2.1. ROMS model of the MAB

ROMS (www.myroms.org) is a hydrostatic, Boussinesq, primitive equation ocean model in widespread use for coastal and mesoscale ocean applications. Shchepetkin and McWilliams (2009) give a thorough review of the elements of the ROMS computational kernel. Among the features that make ROMS attractive for continental shelf applications are a terrain-following coordinate system that can be stretched vertically to better resolve surface and bottom boundary layers, and a formulation of the Equation of State and the density Jacobian that minimize pressure gradient truncation error in the terrain-following coordinates. Together, these enhance the representation of friction, baroclinicity, and the vortex stretching of flow adjacent to steep bathymetry that are fundamental to steering low frequency circulation in the coastal ocean.

The ROMS code offers three different implementations of the 4D-Var method for data assimilation; here we use the incremental strong constraint (IS4DVAR), primal formulation (Moore et al., 2011; Moore et al., 2013; Weaver et al., 2003). In IS4DVAR, a Tangent Linear approximation to ROMS (TL-ROMS) describes the evolution of small perturbations in the nonlinear model trajectory, and the Adjoint to the tangent linear model (AD-ROMS) – forced by perturbations

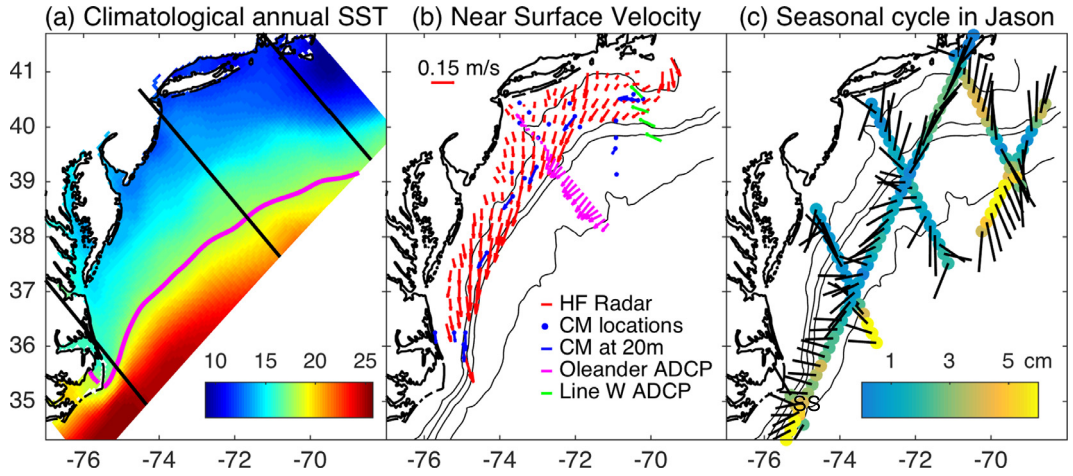

Fig. 2. Observations used in the assimilation and validation. (a) Annual mean sea surface temperature from MOCHA climatology. Solid black lines define northern and southern sub-regions of MAB, and the purple line (18 °C isotherm) the extent of the Slope Sea, used in averages in subsequent figures. (b) Annual mean surface velocity from HF Radar averaged in 30 km bins (red arrows), 20-m depth velocity from current meters (blue arrows), and 35-m depth velocity from *Oleander* ADCP (magenta arrows) and Line-W (green arrows). Blue dots indicate current meters reporting at other depths. (c) Seasonal cycle amplitude (colored circles) and phase (orientation of black lines) for along track Jason altimeter observations. Phase advances clockwise from north starting January 1. Thin black lines in (b) and (c) are 50, 200, 1000 and 3000 m isobaths. (For interpretation of the references to color in this figure legend, the reader is referred to the web version of this article.)

proportional to the model-data misfits – is integrated backward in time to reveal the sensitivities of the control variables (initial, boundary and forcing conditions) to this misfit. The adjoint solution informs a gradient-descent algorithm that adjusts the control variables to minimize a cost function that measures the differences between the observations and their model equivalent, weighted by the observation error. Upon convergence, the final model trajectory represents the "best" analysis of ocean conditions in the sense that it acknowledges all observations and their expected errors, while also imposing the exact solution of the model dynamical equations over the analysis interval (i.e. the strong constraint).

The domain configuration of ROMS used here is the same as that of the "ESPreSSO" (Experimental System for Predicting Shelf and Slope Optics) real-time forecast system operated by MARACOOS (Mid-Atlantic Region Coastal Ocean Observing System) for the MAB (Zavala-Garay et al., 2014). The domain extends from Cape Hatteras to Cape Cod (Figure 1) and from the coast to beyond the shelf break with horizontal resolution of 7 km and 36 terrain-following vertical levels. The model has been used in numerous regional studies related to ecosystems (Hu et al., 2012; Xu et al., 2013), biogeochemical cycles (Mannino et al., 2016), sediment transport (Dalyander et al., 2013; Miles et al., 2015), storm-driven circulation (Miles et al., 2017; Seroka et al., 2017), and underwater acoustics (Lin et al., 2017), as examples. In a comparison of 7 real-time models encompassing the MAB region (Wilkin and Hunter, 2013), no model was more skillful than data assimilative ESPreSSO in capturing MAB circulation.

In this study, the surface forcing air-sea heat and momentum fluxes are climatological annual or monthly means calculated from 10 years (1998 − 2007) of the National Centers for Environmental Prediction (NCEP) North American Regional Reanalysis (NARR) (Mesinger et al., 2006). Coastal freshwater inputs are monthly averages of USGS river flow data adjusted for un-gauged portions of the watershed. Open boundary conditions for temperature and salinity are from the Mid-Atlantic Bight hydrographic climatology of Fleming (2016) described in the next section. Vertical turbulent mixing uses the *k-kl* parameterization implemented by Warner et al., (2005). Prior estimates of velocity and sea level open boundary conditions are assumed, but these are adjusted by the assimilation analysis. Because this is a climatological mean analysis there are no tides. A quadratic drag formulation is used to compute bottom stress, which means that with the omission of tides there is the possibility that mean bottom stress is somewhat underestimated and may be one of the processes compensated for by assimilation adjustments.

2.2. Climatological observational data for assimilation

Several observational data sets have been analyzed to give mean annual and monthly estimates of ROMS state variables (temperature, salinity, velocity and sea level) at locations throughout the domain model. While some, such as temperature and salinity, are in the form of a spatial analysis available at all model grid points, others such as velocity from long-term mooring deployments are at specific locations. The 4D-Var system will spread the information in point observations according to assumed covariance lengths scales informed by the kinematic and dynamic equations embodied in the ROMS circulation model and its adjoint and weighted by respective errors in the observations and model. The provenance of these data and the pre-processing steps taken as described below.

2.2.1. Surface currents from high-frequency radar

A High-Frequency (HF) Radar network operated by MARACOOS has observed surface currents in the MAB since 2009. Radial component data from individual radars are gridded by optimal interpolation into a 6-km resolution vector velocity product with mapping error depending on the number, extent of overlap, and relative direction of the individual radial current observations (Roarty et al., 2010). In preparation for data assimilation, these data were further binned to 30-km resolution, but with velocities with large normalized optimal interpolation mapping errors ignored. The size of the bins was chosen to provide a few "super observations" within the model de-correlation scale of 50 km. A harmonic analysis was applied to derive annual mean (red arrows in Fig. 2b) and seasonal (not shown) climatological values.

2.2.2. Velocity from current meters

Numerous long-term current-meter (CM) deployments have been made in the MAB over the last 35 years, mostly located on the shelf but with several in the Slope Sea. Moored ADCPs offer good vertical resolution, while other moorings might include just one or two observations in the vertical. Utilizing the same set of CM time series of 200 days duration or longer analyzed by Lentz (2008a, 2008b) we computed monthly climatological means by annual cycle harmonic analysis. For ADCP profiles, vertical binning of the data was applied in order to have similar vertical degrees of freedom in the model and observations. In Fig. 2b, current meter locations are indicated by blue dots, and blue

arrows depict the annual average of CM velocity at 20 m depth.

2.2.3. Velocity profiles from MV Oleander ADCP

The container ship *MV Oleander* transits from New York to Bermuda monthly with an ADCP instrument on board that performs autonomous collection of velocity data (Flagg et al., 2006; Rossby and Gottlieb, 1998). Though the data are somewhat noisy, and the ship track does not repeat exactly, nevertheless the very large number of transects allows us to compute a useful climatological mean from data collected in 2005–2009. Individual profiles were binned to equally spaced intervals along the rhumb line, and in the vertical. In each bin, the data that fell more than two standard deviations (2-σ) away from the mean were ignored to remove Gulf Stream ring events that would otherwise bias the mean (Flagg et al., 2006). Harmonic analysis was then performed to obtain monthly climatological profiles of velocity from 35 m to 400 m depth. The magenta arrows in Fig. 2b illustrate the 35 m depth annual currents. These data are the only such direct observational estimate of mean currents in the Slope Sea.

2.2.4. Velocity profiles from Line-W moored ADCP

The Line-W program was a long-term study combining moorings and shipboard observations to investigate the deep limb of the Atlantic meridional overturning circulation (Toole et al., 2011). Vertical profiles of the mean and annual cycle of velocity extracted from data collected at 4 moorings during 2001–2009 (green arrows in Fig. 2b) were assimilated in the model.

2.2.5. Sea surface height anomaly from Jason altimeter

The TOPEX/Jason series of radar altimeter satellites measure sea surface height (SSH) along 6 ground-tracks that traverse the ESPreSSO domain. Data that would ordinarily be rejected by conventional quality control of altimetry in coastal regimes can be reclaimed by judicious application of the data error flags and revised wet tropospheric radar range corrections (Feng and Vandemark, 2011). We extracted 1 Hz along-track (approximately 6 km interval) Jason-1 and Jason-2 data from the Radar Altimeter Database System (RADS; rads.tudelft.nl) for 2006–2012, making range and geophysical corrections to retain data close to land (up to the 25 m isobath). Standard altimetry corrections were applied to remove tides, the inverted barometer effect and other high frequency sea level variability. These data were averaged in 20-km along-track bins, and a 3-month running mean time filter applied. Outliers (based on a 2-σ criterion) were removed. Harmonic analysis was performed on the remaining observations to obtain the climatological seasonal cycle of SSH anomaly (SSHA) (Fig. 2c).

2.2.6. Temperature and salinity climatology

A dataset of hydrographic observations in the MAB drawn from the World Ocean Database (WOD) (Boyer et al., 2009) and augmented by CTD data from the NOAA Northeast Fisheries Science Center (NEFSC) and inner shelf CTD observations acquired by MARACOOS institutions has been mapped to an equal angle 0.05° grid (~5 km) on 57 standard depths by Fleming (2016) using an adaptation of the weighted least squares method of Ridgway et al., (2002). This gridded monthly climatology (MOCHA; Mid-Atlantic Ocean Climatological Hydrographic Analysis) was interpolated to the ESPreSSO model grid for assimilation and adjusted to remove any statically unstable vertical profiles. For illustration, Figure 2a shows MOCHA mean surface temperature. Other features of the MOCHA subsurface temperature analysis are shown in the left-hand panels of Fig. 3, and are discussed in Section 3.

2.3. Climatological 4D-Var assimilation methodology

2.3.1. Prior model estimate

Creating an unbiased prior model estimate greatly assists the success of data assimilation. We accomplished this in a sequence of distinct steps.

In the first step, the ROMS ESPreSSO model configuration described in Section 2.1 was run 12 times (once for each month) initialized with MOCHA temperature and salinity and forced by the respective monthly climatological air-sea fluxes and river inflows (held constant). Boundary sea level and velocity were taken from averages of the 2006–2012 daily analyses of the 1/12° resolution global HYCOM-NCODA data assimilative model (Chassignet et al., 2009; Cummings, 2005). These simulations were run for a period brief enough to let initial transients dissipate and for the velocity and sea level to approach dynamic equilibrium without allowing temperature and salinity to deviate too much from the climatology. For summer months, this adjustment was largely complete within a week, so we averaged the second week of a 2-week simulation to obtain a prior estimate for those months. For winter months, this approach did not converge satisfactorily, with unrealistically large currents arising at the shelf-break during the dynamic adjustment. So instead each winter month was initialized with MOCHA from the prior month, then run changing the boundary conditions and surface forcing gradually over 45 days, with the average of the last 30 days of simulation retained as a monthly estimate. Next, these initial 12 estimates were averaged to produce a prior solution for an IS4DVAR analysis that assimilated the annual mean climatology data sets described in Section 2.2. The final step was to re-run the 12 climatological monthly forward model runs replacing HYCOM-NCODA sea level and velocity open boundary and initial conditions with the annual mean adjusted values. This was done in order to have a better balance between all the fields at initialization of the forward model. This approach is admittedly ad hoc, but it should be recalled that the objective is merely to obtain a reasonable “first guess” to be adjusted subsequently by data assimilation.

2.3.2. Error hypothesis

IS4DVAR requires a prior estimate of the model background error covariance for initial, boundary and air-sea forcing conditions. We specify these as a univariate correlation matrix scaled by standard deviations and spatial decorrelation scales estimated from the mesoscale variability in a multi-year forward run (i.e. no DA) of ESPreSSO. The standard deviation in surface fluxes was halved to achieve better stability in the assimilation. The initial condition error de-correlation scale is 50 km in the horizontal, and 50 m in the vertical; boundary condition de-correlation scale is 100 km in the horizontal and 100 m in the vertical; surface forcing de-correlation scale is 100 km.

An estimate of the observation errors is also required, but this is a difficult choice for averaged climatological data sets. Observational errors should be small enough to keep the model as close as possible to a steady climatological solution, yet large enough to allow the minimization algorithm to converge to a dynamically balanced solution. We chose to set observational error for temperature and salinity to be 1/3 of the assumed model background error at the surface, and to increase this to the mean model error over 150 m depth. Adjacent to the continental slope, the error estimate for climatological temperature and salinity was elevated to prevent reintroducing unphysical currents near the shelf break.

Velocity and SSH observational errors were set proportional to the standard deviation within each of the spatial averaging bins described above, scaled to make the mean of the errors equal to the 1/10 of the mean model background standard deviation at the corresponding observation locations.

2.3.3. Analysis procedure

IS4DVAR iterates forward and backward in time within an analysis interval – here we use 2 days. Since we seek a steady climatological result, time evolution of the solution over the interval is penalized by repeating the observations numerous times within the assimilation window: temperature and salinity observations are repeated every 4 hours, while velocity and SSH are repeated every 30 minutes. An average of the converged model solution over the assimilation window

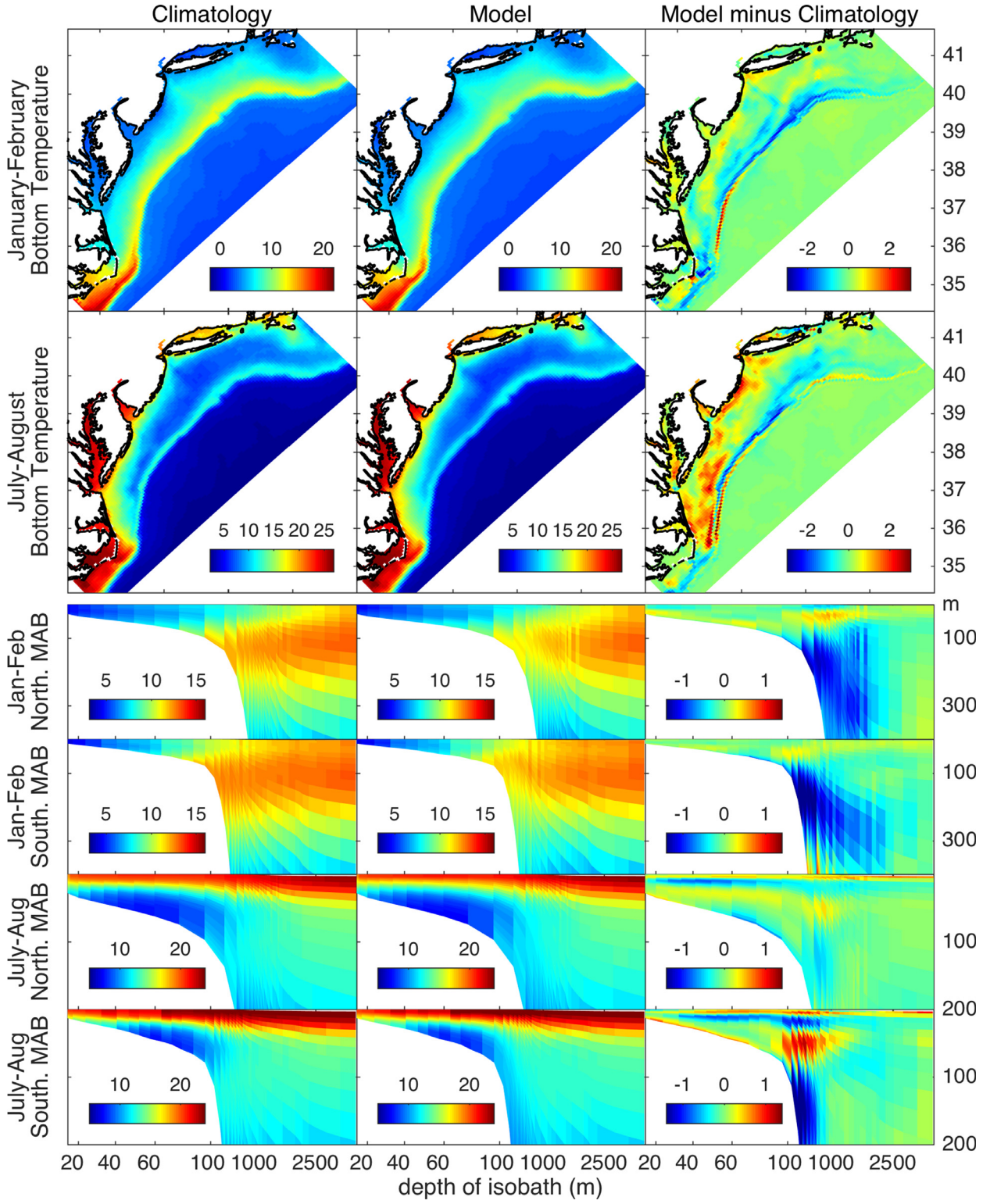

Fig. 3. Temperature from MOCHA climatology (left column), ROMS TSV (center), and their difference observed minus model (right). Vertical cross-sections in the lower panels are along-isobath averages within the northern and southern sectors defined in Fig. 1a, and are plotted as a function of depth (m).

becomes the completed analysis.

Model-data misfit decreased when boundary conditions and surface forcing were added to the control variable set, in addition to the model initial conditions. In particular, adjusting the surface flux was instrumental in better fitting observations in the surface mixed layer, although the surface wind stress and heat flux after assimilation were not particularly realistic. Adjustment of boundary conditions did not substantially improve the assimilation results.

We are not solving the *time-averaged* ROMS governing equations by this approach, and strictly speaking there is therefore a conceptual error in the dynamical model. In strong constraint assimilation there is no explicit account of model errors; that would require a “weak constraint” formulation (Sasaki, 1970). By seeking initial and forcing conditions that pull the solution of the nonlinear model toward a steady model

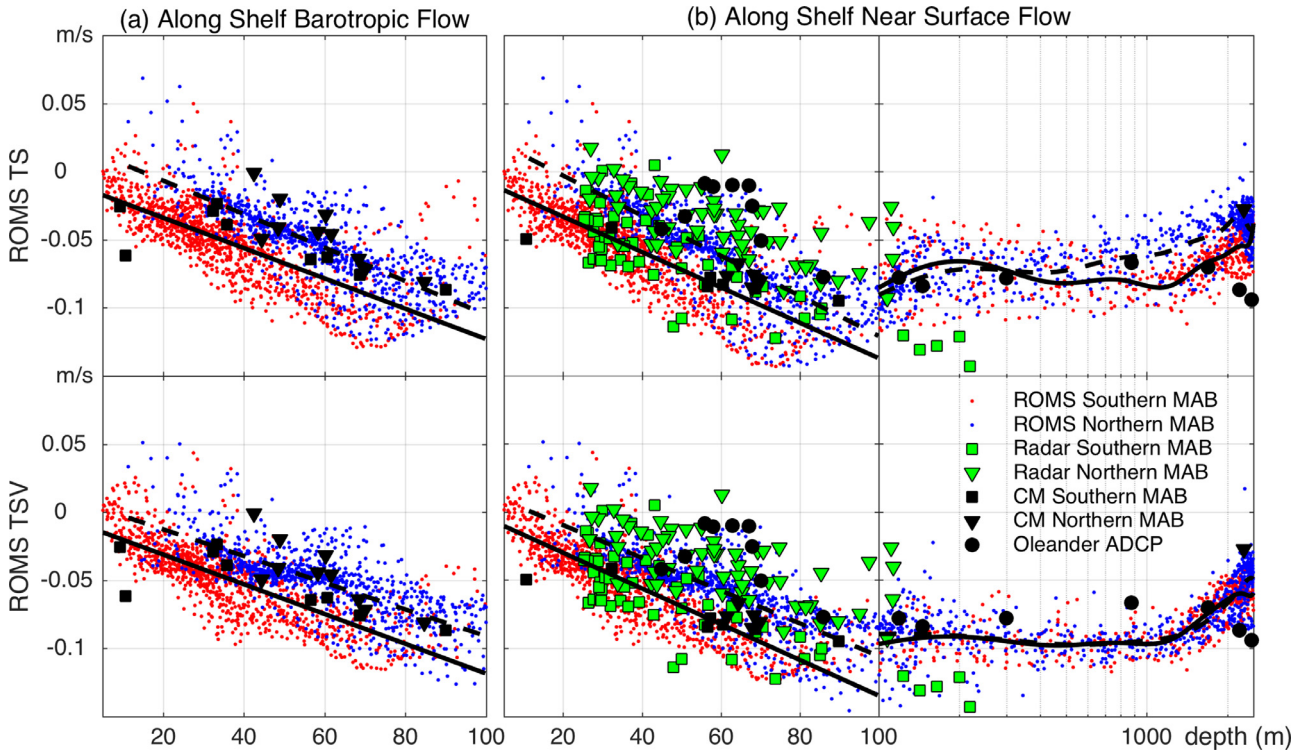

Fig. 4. (a) Depth average and (b) surface to 40 m vertical mean of along shelf velocity in ROMS TS (top row) and TSV (bottom row) experiments (small red and blue dots) compared to current meter observations (black squares and triangles), HF-radar near surface observations (green squares and triangles), and 35 m depth ADCP measurements from Oleander (black circles). Comparisons are grouped by northern and southern MAB sectors defined in Fig. 1a. Heavy black lines show least squares fit to model values in the southern (solid) and northern (dashed) MAB sub-regions. (For interpretation of the references to color in this figure legend, the reader is referred to the web version of this article.)

trajectory over the analysis window we are not allowing for the residual time trend that would be a small but non-zero term in the monthly averaged dynamical equations. This is clearly a shortcoming of our model design, but a more precise configuration would require a time-averaging observation operator in adjoint ROMS and a complete implementation of weak constraint assimilation such as the representer method of Bennett (2002). These features are not presently available to us in ROMS 4DVAR. The improved outcome when surface fluxes are adjusted perhaps reflects that the climatological model set-up needs the opportunity to accommodate model error, and diverts this (somewhat erroneously) to adjusting the surface forcing.

We acknowledge this methodology is heuristic, so should be judged by its ability to deliver a useful solution for the intended purpose, namely, computing 3-D ocean circulation analyses that are in near dynamic balance, steered by coastal bathymetry, and close to observed features of the long term mean ocean state where those are available. This evaluation is the subject of Section 3 where we contrast the results from assimilation experiments with successively more comprehensive observational constraints.

2.3.4. Three different assimilation experiments

To test the relative influence of various types of observations for constraining climatological circulation, several different monthly assimilation experiments were conducted. In all cases, initial and boundary conditions, monthly surface forcing, and monthly average observational data as described above were used.

In the first experiment, denoted ROMS TS, only the temperature and salinity climatology from MOCHA was assimilated. In the second experiment, we started with the same set of prior solutions as before, but in addition to temperature and salinity we assimilated velocity from HF-radar, moored CM and *Oleander* ADCP. This is experiment ROMS TSV. These two experiments examine how well climatological in situ observations constrain the circulation in the absence of satellite-based SSH climatology.

ROMS IS4DVAR requires observations that correspond to model state variables, and therefore we cannot readily assimilate *anomaly* SSH because ROMS sea level is effectively *absolute* dynamic topography (MDT included). However, since ROMS TSV provides an MDT estimate, we add this to monthly Jason SSH anomaly data and conduct a third assimilation experiment, denoting this case as ROMS TSVH.

3. Results

3.1. ROMS TS and ROMS TSV results

3.1.1. Annual mean and seasonal temperature

Fig. 3 shows aspects of the MOCHA temperature climatology, the ROMS TSV analysis, and their difference. Views include winter (top row) and summer (second ro) bottom temperature on the shelf, highlighting a well-defined summertime subsurface “cold pool” (Houghton et al., 1982) of waters less that 9 °C on the shelf. To characterize the overall pattern of vertical and across-shelf stratification, along-isobath average winter and summer temperature for the shelf and slope are shown in the lower panels of Fig. 3 for northern and southern sub-regions defined in Fig. 2a that echo quasi-2D climatological dynamical analyses of the MAB (Lentz, 2008a; Linder and Gawarkiewicz, 1998).

Temperature in the ROMS TS experiment (not shown) has a slightly better fit than in ROMS TSV, but both fit the climatological temperature and salinity well, as is to be expected since the data were assimilated. The adjusted bottom temperature departure from climatology is greatest in the summer when the vertical decorrelation scale in the background error causes some loss of the sharp summer thermocline that is resolved well by the fine standard depth resolution in MOCHA.

In addition to the strong vertical thermal stratification and subsurface cold pool on the shelf, the assimilation retains the bowl of warm subtropical water offshore in the Slope Sea. The largest deviation from climatology occurs at the shelf break where the assimilation adjusts temperature and salinity to introduce more steeply sloping isotherms in accordance with the dynamics of the shelf-break front.

3.1.2. Annual mean velocity

While ROMS TS and TSV experiments are similar in terms of temperature and salinity, they differ somewhat in their estimates of velocity. Fig. 4 shows along-shelf depth-average velocity as a function of ocean depth in ROMS TS and TSV experiments grouped by northern and southern sub-regions of the MAB defined in Fig. 2a (values in the estuaries and bays are not plotted) and compared to values estimated by Lentz (2008a) from current meters.

On the shelf, inshore of the 100-m isobath, model depth-averaged along-shelf velocity is in reasonable agreement with current meter data in the northern MAB, but somewhat less so in the southern MAB. However, it should be noted that the small dots in Fig. 4 are distributed throughout the shelf, and the handful of current-meter deployments from which depth-averaged velocity was estimated may not be representative of the model spread. Model currents increase with water depth with a regression slope of $-0.08\ \mathrm{cm\ s^{-1}\ m^{-1}}$ and an intercept of $-1.2\ \mathrm{cm\ s^{-1}}$, values that are close to $-0.07\ \mathrm{cm\ s^{-1}\ m^{-1}}$ and $-1.8\mathrm{cm\ s^{-1}}$, respectively, that Lentz (2008a) estimated from CM data. Surface currents on the shelf are fit well in both experiments (Fig. 5). Depth-average and surface currents in ROMS TSV are slightly closer to the observations by virtue of their being assimilated.

The assimilation of velocity data has moderate impact on the inner shelf, but tends to decelerate the along-shelf current on the outer shelf and near the shelf-break. In deeper water beyond the shelf-break there are no observations over the full water column to constrain depth-average velocity, but limited surface current data from HF-radar in the southern MAB, and upper water column data from *Oleander* ADCP, show that with assimilation the flow is accelerated along the continental slope (water depths 100–400 m) and decelerated in the deep Slope Sea (water depths > 1000 m) to bring ROMS TSV into better agreement with the observations.

These influences of the velocity assimilation are also evident in Fig. 5, which presents a map view of the surface current observations, model results, and their difference. In ROMS TS the surface flow in the central MAB is too fast and too strongly aligned with isobaths. In ROMS TSV, assimilation of HF-radar and current meter observations is helpful in turning the surface flow offshore, while assimilation of *Oleander* data is instrumental in making the flow more uniform throughout the Slope Sea. In the far southern MAB the along-shelf flow weakens in ROMS TS when in fact the convergence of isobaths sustains the strong current there, even as much of the transport turns offshore. Assimilation restores the magnitude of the current on the shelf as the flow approaches Cape Hatteras. The root mean square error between model and all velocity observations decreases from $0.049\ \mathrm{m\ s^{-1}}$ in ROMS TS to $0.031\ \mathrm{m\ s^{-1}}$ in ROMS TSV and $0.025\ \mathrm{m\ s^{-1}}$ in ROMS TSVH.

The vertical structure of velocity is shown in Fig. 6, where again the solution is averaged along isobaths and plotted as a function of water column depth. In water shallower than 100 m both solutions show southwestward flow (out of the page) that intensifies moving seaward from the coast to the shelf-break. In ROMS TS (Fig. 6, top row) there is a reversal of the along-shelf bottom flow immediately beyond the shelf-break near 150 m water depth that we believe to be unrealistic. This erroneous northward flow occurs throughout the MAB but is most pronounced in the southwest, where it allows the Gulf Stream to encroach onto the southern MAB shelf. When velocity data are assimilated in ROMS TSV (Fig. 6, bottom row) this undercurrent is greatly diminished. The adjustment of ROMS TSV to show weaker northward flow at the seafloor at the 150-m isobath is accompanied by local strengthening of the surface current. This suggests the vertical velocity shear and hence thermal wind density gradient are not appreciably altered, and that 4DVAR has accommodated the added velocity data by modifying the sea level gradient. Over the upper 400 m of the water column where *Oleander* data are present the ROMS TSV comparison naturally improves, and these changes in velocity propagate into the deeper Slope Sea.

It has been suggested (Lentz, 2008a; Zhang et al., 2011) that the across-shelf circulation in the MAB has a two-layer structure in the inner shelf with offshore flow at the surface and on-shore flow below; and a three-layer structure in the outer shelf with offshore flow at the surface and bottom, and on-shore at mid-depths. The presence of a mean geostrophic on-shore flow at mid-depths demands there be an along-shelf pressure force due largely to a sloping sea level. The right column in Fig. 6 shows the along-isobath averaged across-shelf velocity and along-shelf pressure force expressed in terms of an equivalent sea level gradient. When assimilating temperature and salinity alone (ROMS TS), the model did not generate significant across-shelf flow in the inner shelf, and on the outer shelf the across-shelf circulation was rather weak. In ROMS TSV, we recover the across-shore circulation in the inner and outer shelves as described by Lentz (2008a) and Zhang et al., (2011). On the inner shelf, the model has $0.5\ \mathrm{cm\ s^{-1}}$ offshore surface currents, weak on-shore flow, and upwelling through the water column. On the outer shelf, the across-shelf flow increases to $\sim 1\ \mathrm{cm\ s^{-1}}$ at the surface, $0.2\ \mathrm{cm\ s^{-1}}$ on-shore through the mid-depth range with weak down-welling, and $\sim 2\ \mathrm{cm\ s^{-1}}$ off-shore in the bottom Ekman layer. Upwelling of about $0.01\ \mathrm{mm\ s^{-1}}$ is reported in the inner portion of shelf-break (between 100-m and 1000-m isobaths), which is consistent with the results of Zhang et al., (2011). In conjunction with the strenghtened across-shore circulation there is an increase in along-shore pressure gradient, consistent with Lentz' result that this force is significant in the along-shelf momentum balance.

3.1.3. Seasonal cycle of velocity

The seasonal cycle of near surface velocity is shown in Fig. 7 in the form of ellipses computed by harmonic analysis for both the model and observational monthly fields, and plotted at the observation locations. While velocity data from the various observational platforms agree reasonably well with each other in the annual mean (Fig. 5a), there are some considerable differences between platforms in seasonal variability (Fig. 7a). Current meter data show the largest amplitude of seasonal variability ($\sim 5\ \mathrm{cm\ s^{-1}}$). HF-radar observes smaller seasonal change of about 1 to $5\ \mathrm{cm\ s^{-1}}$, with the largest variability close to the coast. Seasonal variability is greatest toward the south, near Chesapeake Bay and Cape Hatteras. The magnitude of *Oleander* seasonal variability on the shelf agrees with HF-radar, but is out of phase with it; note that HF-radar captures the flow at ~ 2 m depth (Ullman et al., 2006) whereas the shallowest reliable Oleander ADCP range bin is 35 m below the sea surface. In the Slope Sea, *Oleander* exhibits larger variability up to $15\ \mathrm{cm\ s^{-1}}$. There are insufficient data at Line-W to obtain a meaningful seasonal cycle.

The seasonal variability of velocity in ROMS TS is not particularly realistic, with large ($20\ \mathrm{cm\ s^{-1}}$) discrepancies in the southern MAB (Fig. 7b). This is unsurprising given that only temperature and salinity are assimilated and serves to emphasize that a diversity of observation types is required for effective multi-variable state estimation by data assimilation.

The seasonal cycle in ROMS TSV (Fig. 7c) is much more similar to the observations, but still with some differences. In particular, while trying to fit the two somewhat conflicting HF-radar and near surface CM data sets, the model has practically ignored the seasonal cycle in the CM in favor of HF-radar seasonal cycle. In the Slope Sea, where *Oleander* is the only source of data, the model fits the observed seasonal cycle well. This apparent preference of HF-radar over coincident CM data may indicate imperfect observation error estimates that give excessive relative weight to HF-radar, or an imperfect background error model with overly long vertical covariance scale that connects velocity

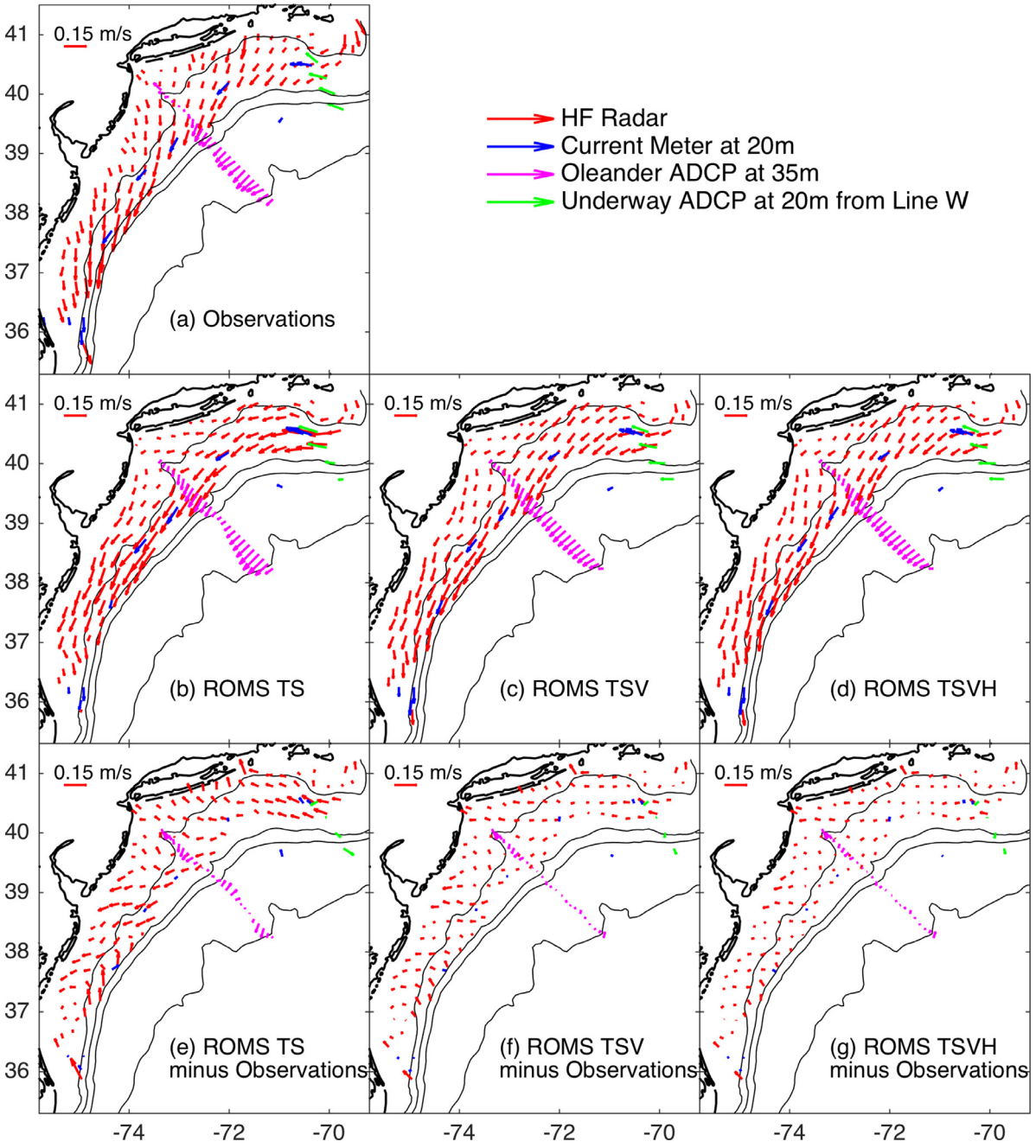

Fig. 5. Comparison of annual mean velocity from ROMS TS, TSV and TSVH experiments with measured velocity from HF-radar (red arrows), 35-m depth Oleander ADCP (magenta arrows), current meter at 20 m depth (blue arrows), and Line-W ADCP at 20 m depth (green arrows). Thin black lines show 50, 200, 1000 and 3000 m isobaths. Model velocities are interpolated to the same locations as observations and shown in the same color. (For interpretation of the references to color in this figure legend, the reader is referred to the web version of this article.)

in the mixed layer to the underlying flow when these are in fact largely decoupled.

3.1.4. Mean dynamic topography and seasonal SSHA variability

The ROMS TSV solution gave an annual mean velocity and temperature analysis that compared well with the data in most of the domain and was constrained by ROMS model physics. The corresponding model sea level solution represents an MDT that is dynamically consistent with the other fields, and whose estimation is a key objective of our assimilation project. Comparing the ROMS MDT results to the independent AVISO MDT (Fig. 8) we see that model and AVISO are broadly similar in the Slope Sea and Gulf Stream. Some modest variation between the two is to be expected because of the different methods used, but also because AVISO is based on hydrographic and drifter data from 1993–2012 whereas our solution uses hydrographic climatology for which 50% of the data were acquired before 1993 (Fleming, 2016). To attempt an MDT analysis based strictly on observations acquired in the TOPEX/Jason altimeter era we would also have to exclude more than half the moored current meter velocity data, and for most of the MAB HF-radar data are available only in the last 5 years of the 1992–2012 period.

Though the two MDTs are similar offshore, they differ dramatically on the shelf where the majority of velocity observations are located and where bathymetry and coastline strongly steer the flow. Assimilation of

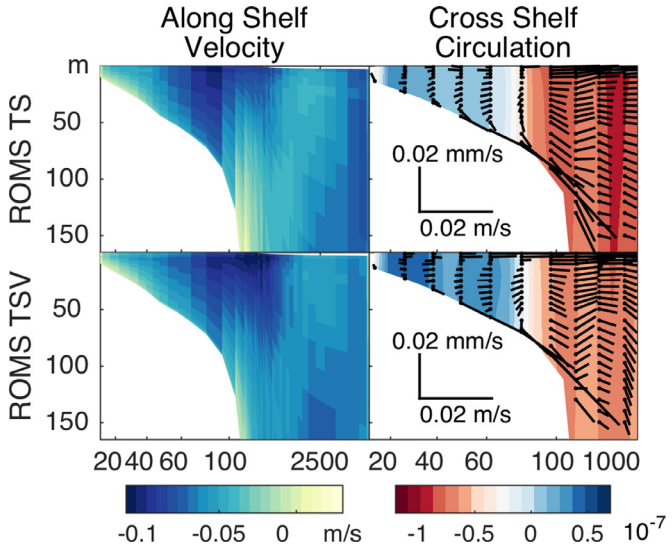

Fig. 6. Left: Along-shelf horizontal velocity. Right: Across-shelf circulation (black sticks) and along-shelf pressure gradient (color) normalized to equivalent sea level slope. Top row: ROMS TS. Bottom row: ROMS TSV. All values are averaged along isobaths over the two MAB sectors and within the Slope Sea as defined in Fig. 1a.

temperature and salinity provides information crucial to determining details of the MDT in the Slope Sea and in the Gulf Stream, while velocity data add additional constraints on the shelf and upstream of the *Oleander* line. The strong constraint of the data assimilation introduces dynamically sensible MDT on the shelf. The shelf sea level pattern is characterized by a steep across-shelf slope of some 10 cm in 100 km that is quite uniform throughout the MAB, and which is consistent with the predominantly geostrophic balance of the mean along-shelf flow (Lentz, 2008a).

The amplitude and phase of seasonal sea level variability is shown in Fig. 9, which may be compared to Jason SSHA data in Fig. 2c. Variability in the Slope Sea is associated with a slow seasonal meander of the Gulf Stream, but since this is close to the model boundary we do not put great faith in the result. Of more interest is the continental shelf, where in the northern MAB variation over the year is about 4 cm with a maximum in winter, though the comparison to Jason suggests the amplitude of variability may be underestimated. In the southern MAB there is little variability at all in the ROMS TSV results. In terms of phase, along-track altimetry data agree with the ROMS TS and TSV solutions in the Slope Sea and the northern and central MAB shelf, but disagree in the southern MAB and in the Gulf Stream area.

The ROMS TS solution suggests that the fit between modeled and observed SSHA comes mostly from assimilating temperature and salinity. The added assimilation of velocity data only improves the phase of the sea level cycle in the central and northern MAB. To bring modeled

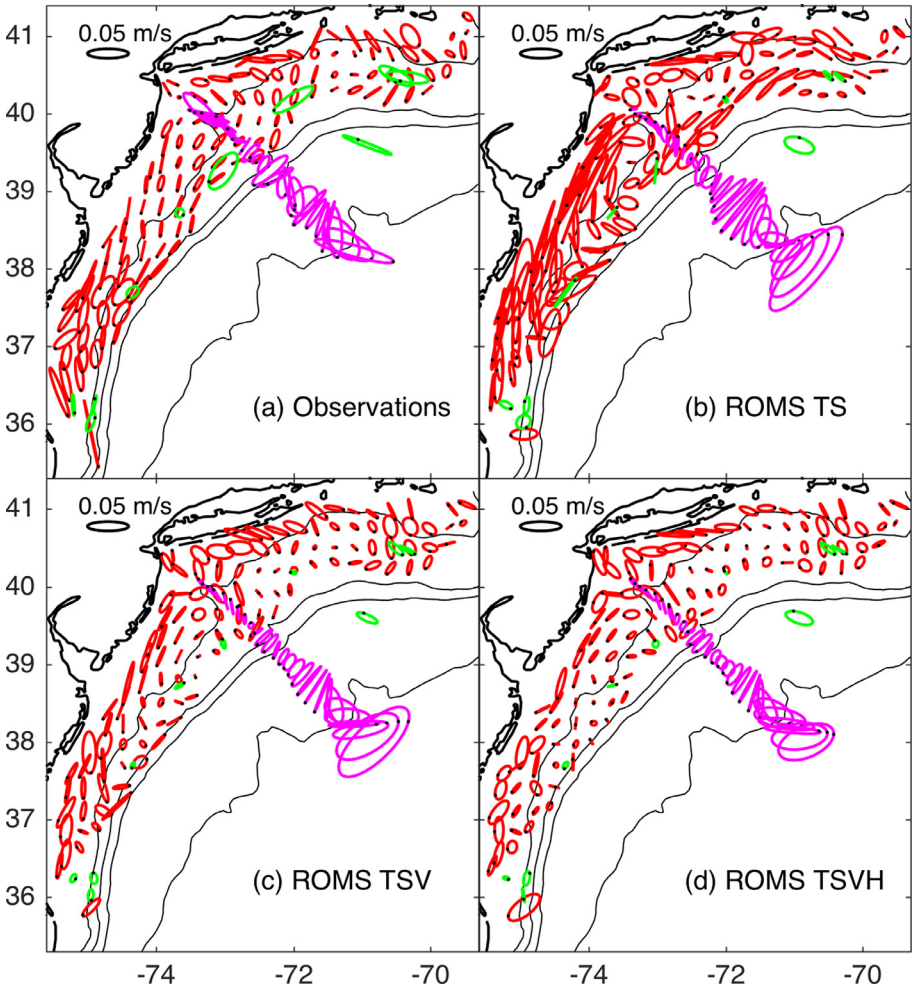

Fig. 7. Comparison of near surface velocity seasonal cycle from ROMS TS, TSV and TSVH experiments with observed velocity variability from HF-radar (red ellipses), 35-m depth Oleander ADCP (magenta ellipses), and current meters at 20 m depth (green ellipses). Black dots on the seasonal ellipses indicate the phase corresponding to January 1. Thin black lines show 50, 200, 1000 and 3000 m isobaths. Model velocities are interpolated to the same locations as observations and shown in the same color. (For interpretation of the references to color in this figure legend, the reader is referred to the web version of this article.)

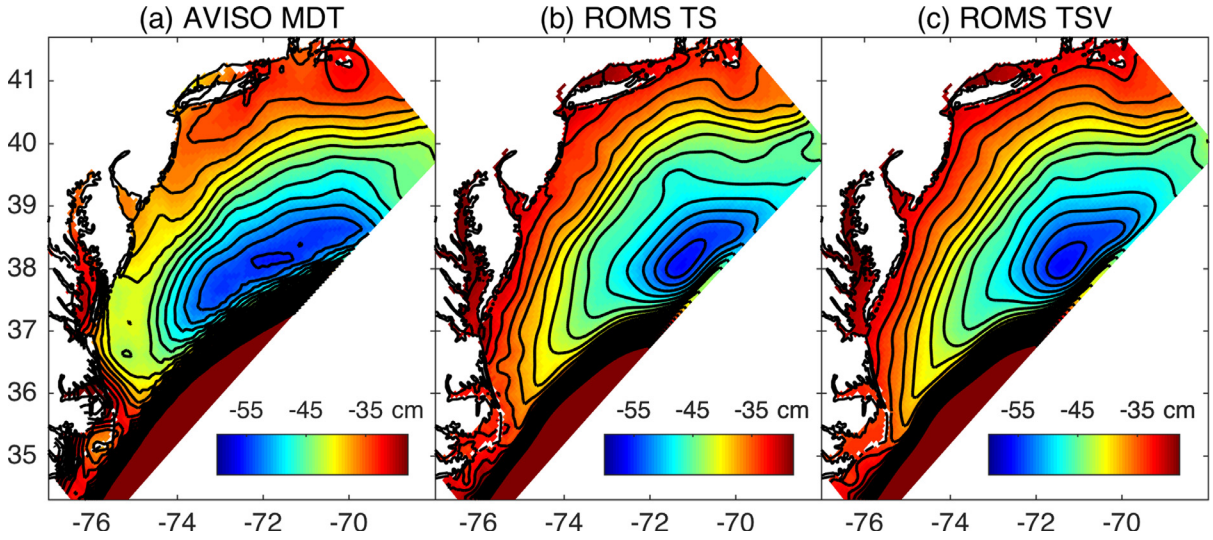

Fig. 8. Mean Dynamic Topography from (a) CNES-CLS13 AVISO MDT (same data as Fig. 1a), (b), ROMS TS and (c) ROMS TSV. All fields have the same spatial mean.

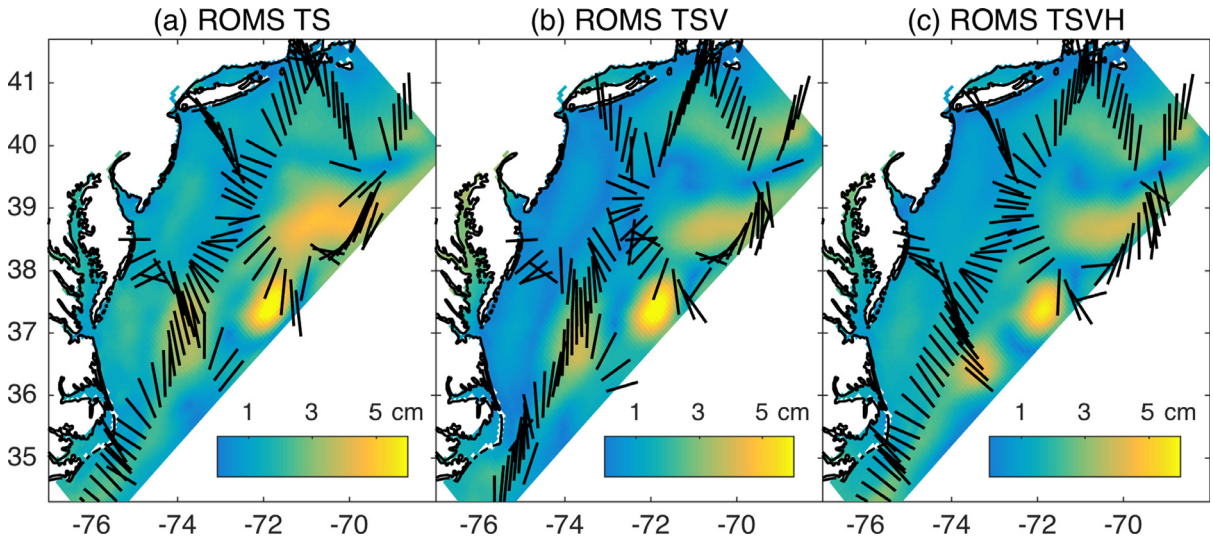

Fig. 9. Seasonal cycle amplitude (color) and phase (orientation of black lines) for the three ROMS experiments (a, b, c). Phase advances clockwise from north starting January 1. Corresponding Jason altimeter observations are shown in Fig. 2c.

sea level variability into better agreement with satellite SSHA we add altimeter data into the monthly assimilation analyses in the next experiment.

3.2. Assimilation of altimeter along-track SSHA

Thus far we have not assimilated satellite altimeter SSHA data because we need to know MDT in order to formulate observations (MDT + SSHA) that correspond to the ROMS sea level state variable. AVISO MDT is unsatisfactory for this purpose on the shelf. However, we now have a good estimate of MDT from the ROMS TSV solution, so we have conducted a further set of monthly assimilation experiments in which MDT added to Jason SSHA comprise a set of SSH observations to augment the suite of temperature, salinity and velocity data. We denote this set of monthly assimilations as ROMS TSVH. All other parameters of the assimilation are kept the same.

Changes with the addition of altimetry are not dramatic, but they are consistently an improvement. With SSH assimilation, the modeled amplitude and phase of the seasonal cycle of sea level variability in the southern Slope Sea and southern MAB shelf (Fig. 9c) is brought into agreement with observations, as are the seasonal velocity ellipses in the central Slope Sea as observed by *Oleander*, but there is no significant change, for better or worse, in the variability in the northern MAB. Nor, overall, are there any significant changes in the mean velocity fit (Figs. 5f and 5g differ little) and we retain the MDT from ROMS TSV as our best estimate of annual mean ocean conditions in the MAB.

4. Features of the mean ocean circulation in the MAB

As we have noted earlier, 2-D studies (Lentz, 2008a; Linder and Gawarkiewicz, 1998; Zhang et al., 2011) have characterized across-shelf circulation on the outer shelf as being predominantly offshore in the surface and bottom Ekman layers, with compensating on-shore flow in a geostrophic interior. In the full 3-D case these transports need not balance locally, but may instead be matched by divergence of the along-shelf transport. Using the annual mean result of the ROMS TSV experiment, we examine how transports vary spatially along-shelf.

We computed the across-isobath component of flow by taking the inner product of the velocity with the gradient of bathymetry normalized to a unit vector, i.e. $\nabla h/|\nabla h|$. A simple 9-point 2-D triangular filter was applied to the depth, h, prior to computing ∇h to suppress noisiness in the calculation arising from depth variations on length scales of order

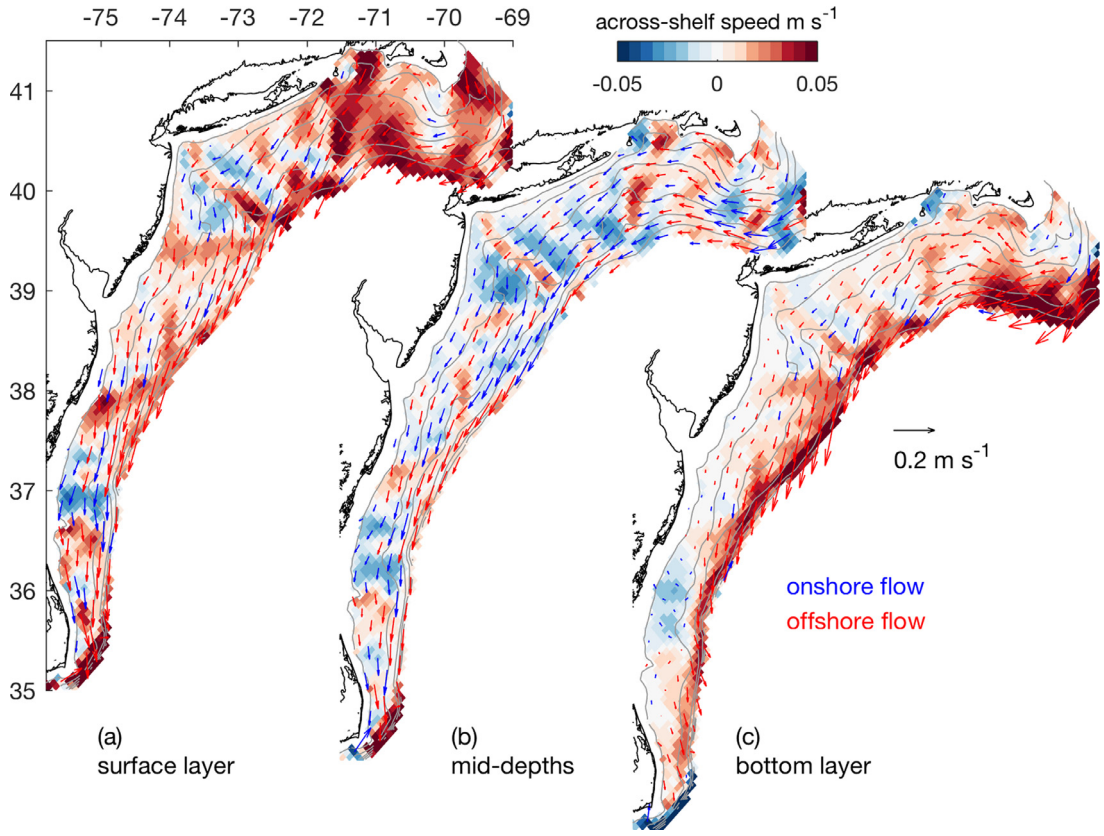

Fig. 10. Annual mean velocity at (a) the surface, (b) vertically averaged from 5 m below surface to 5 m above seafloor, and (c) at the bottom. Colors show magnitude of component of flow in the local across-isobath direction. Blue shades are onshore, red shades are offshore. Vectors are similarly color coded by sense of across-isobath flow; for clarity, vectors for only every 3rd grid cell are plotted. Light grey lines are isobaths from 20 m to 95 m at 15 m intervals.

20 km or less. The calculation was made separately for flow at the sea surface, at the bottom, and vertically averaged over the portion of the water column from 5 m below surface to 5 m above the seafloor so as to exclude boundary layer circulation from the mid-depths result. The across-shore component of current is depicted by color shading in Fig. 10, with warm (cool) colors indicating offshore (onshore) flow. Arrows show the vector velocity in each layer average, color coded by the sense of the across-shore component for emphasis. Only vectors for every 3rd model cell are plotted, but the color shading shows that patterns are coherent on length scales spanning several grid cells. In accord with the 2-D studies there is a preponderance of offshore flow in the boundary layers, and onshore flow in the interior, but there is considerable local variability in the sense of the across-isobath flow as the circulation wends its way southwestward throughout the MAB.

Some trends emerge in this spatial variability if we focus on the flow at an isobath on the outer shelf. Fig. 11 shows conditions along a path coinciding with the 65 m isobath, bracketed by across-shelf transects that connect the isobath to the coast. Fig. 11c therefore depicts across-shelf flow where the transect follows the isobath, but is augmented with strong along-shelf flows that are into and out of the control volume at the two ends of the transect. These saturate the color bar, so contours of 0.05 and 0.075 m s^{-1} are added. The abscissa of Fig. 11a,c,e is distance from the southern end of the path, with green markers corresponding to those in Fig. 11b that delineate 3 southern, central and northern sub-regions that are averaged in Fig. 11d,f.

In the surface and bottom boundary layers, flow is offshore at the 65-m isobath throughout the MAB, but to varying intensity. The interior flow is quite barotropic, consistent with Lentz' (2008a) assertion that following an isobath there is insufficient along-shelf variation in density to sustain a thermal wind vertical shear in the across-shelf current. Rather, geostrophic balance of the across-shelf interior flow must be achieved with an along-shelf tilt to the sea level. This across-shelf interior flow is not consistently onshore as might be supposed from the 2-D studies, but changes sign frequently as the flow gently meanders across isobaths. To quantify this, we plot depth-integrated transport streamfunction along the section in Fig. 11c. There is a net inflow of 0.136 Sv through the northern end section and outflow of 0.109 Sv at the southern extremity. Between these limits there is convergence and divergence of the across-isobath flow that accumulates to the moderate net loss of 0.03 Sv, or 20% of the northern inflow.

Considering averages in three approximately 200-km long sub-sections (Fig. 11d,f) we see that the northern and central sectors are indeed "Lentz-like" ; there is outflow in the boundary layers and inflow in the central water column, and these are approximately volume conserving (inspect the values of streamfunction at the green markers in Fig. 11c).

The along-shelf current (Fig. 11e) is everywhere southward, but accelerates as the flow moves toward the southern end of the 65-m isobath section. Because this flow reaches the seafloor, it drives increasingly strong offshore transport in the bottom Ekman layer in the southern sector (Fig. 11d). But the greatest difference compared to the northern sub-sectors is that the interior flow is now directed offshore at all depths. This is a region of significant leakage of the southward volume flux to deeper offshore waters, whereas the north is not.

These features of the circulation are not peculiar to the 65-m isobath. In Fig. 10b we see that anomalously onshore and offshore flow is organized into largely across-shelf coherent bands indicating that where the current meanders horizontally it does so in an across-shelf coordinated fashion. We speculate that this meandering is the response of the depth-integrated flow to vortex stretching induced by variations in the bathymetry on along-shelf scales that are too short for the depth-integrated potential vorticity to have adjusted so as to remain parallel to isobaths. Exploring this conjecture would best be pursued by analysis

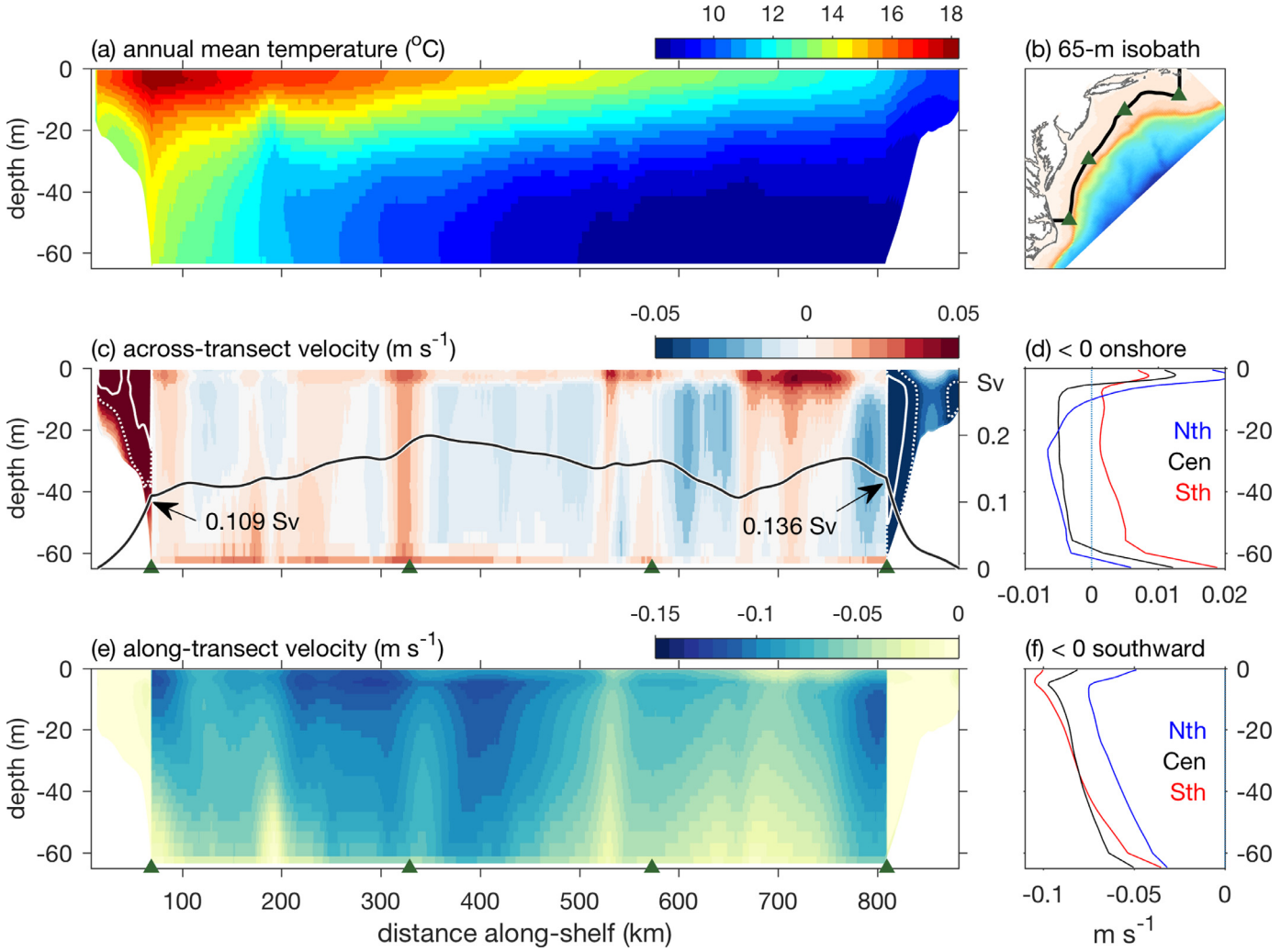

Fig. 11. ROMS TSV annual mean conditions on a transect (black line in (b)) along the 65 m isobath and across-shelf end sections. (a) Temperature, (c) across-transect velocity, and (e) along-transect velocity. Panels (d,f) show along-shelf averages of (c,e), respectively, in three sub-regions (north, central and south) between the green markers in (b). In (c), white contours in end sections are 0.05 m s^{-1} (dotted) and 0.075 m s^{-1} (solid), and the black solid line is the depth-integrated across-transect transport stream function.

of a freely-running model constrained by our mean solution only as open boundary conditions and unencumbered by data assimilation that upsets exact closure of the time averaged momentum and vorticity equations.

A change in along-shelf dynamical balance that contributes to this offshore flow on the southern outer shelf becomes apparent if we plot MDT following selected isobaths (Fig. 12). A positive slope indicates sea level is increasing toward the north. On the inner and mid shelf (35-m and 50-m isobath) sea level slopes of 4.5–5.6 $\times 10^{-8}$ are only moderately higher than the value 3.7 $\times 10^{-8}$ estimated by Lentz (2008a), which his conceptual model assumed to be spatially uniform. However, we find that in the southern MAB seaward of the 50 m isobath there is a marked change in sea level tilt such that it opposes the southward current on the outer shelf. (Even inside the 50 m isobath there is a local reversal in tilt before the slope continues its decrease approaching Cape Hatteras.)

It is difficult to discern in Fig. 10b because the isobaths are so close in this part of the shelf, but the flow in this region is consistently directed offshore at all depths. If this sea level gradient were balanced by a uniform barotropic across-shelf geostrophic flow it would drive 0.07 Sv of offshore transport across the 65-m isobath in the southern sub-region in Fig. 11c, which unsurprisingly is very close to the volume loss in this sector suggested by the streamfunction calculation.

Returning to the matter of across-shelf variation in the along-shelf sea level tilt, our results are at odds with the idealized 2-D modeling study of Zhang et al., (2011) that suggested this tilt increases dramatically approaching the coast, reaching as much as 1.3 $\times 10^{-7}$ in the annual mean, whereas we see only one third this magnitude. Recalling that Lentz (2008a) assumed no across-shelf variation in slope, and focusing on the more "Lentz-like" northern MAB where the mass balance appears to be approximately 2-D, we actually see a modest increase (Table 1) in the along-shelf sea level slope going from mid-shelf (35-m isobath) to the outer-shelf. However, a clear point of agreement with Zhang et al., (2011) is a pronounced seasonal cycle in the sea level tilt: greatest in winter and least in summer, though the seasonal transitions correspond less well. This being a regional, diagnostic analysis, we are none the wiser as to the dynamical origins of this variability.

5. Summary

We have presented a mean 3-dimensional circulation analysis for the Mid-Atlantic Bight computed by variational data assimilation in a regional ocean model. The data assimilated comprise climatological monthly mean ocean state conditions (temperature, salinity, velocity, and sea level anomaly) derived from historical observations from all available platforms in the region. The analysis was conducted for

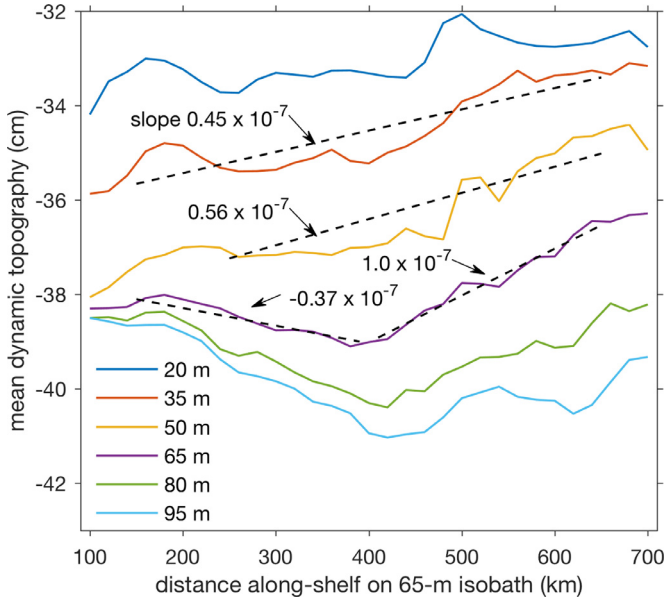

Fig. 12. Mean Dynamic Topography following selected isobaths in the MAB. Abscissa coordinate is the same as in Fig. 11. Dotted lines are linear fits over the along-shelf extent indicated by each line, annotated with the corresponding slope.

Table 1
Average along-shelf sea level slope following selected isobaths in the MAB. Regions over which the slopes are computed are the same as those defined in the text for Fig. 12, and the Annual values tabulated below match the annotations in Fig. 12.

	Isobath			
	35 m	50 m	65 m	
Season			Southern MAB	Northern MAB
Winter	0.664×10^{-7}	0.875×10^{-7}	-0.021×10^{-7}	1.66×10^{-7}
Spring	0.672×10^{-7}	0.673×10^{-7}	-0.395×10^{-7}	0.956×10^{-7}
Summer	0.208×10^{-7}	0.249×10^{-7}	-0.468×10^{-7}	-0.0049×10^{-7}
Fall	0.257×10^{-7}	0.424×10^{-7}	-0.612×10^{-7}	1.35×10^{-7}
Annual	0.451×10^{-7}	0.555×10^{-7}	-0.374×10^{-7}	0.992×10^{-7}

annual mean, and monthly climatological mean conditions. In the latter case, the seasonal cycle in satellite altimeter sea surface height anomaly was included as a further data constraint, exploiting the mean sea level estimate from the initial data assimilative analysis. The model was forced by climatological mean river inflows and air-sea fluxes, but with the data assimilation system adjusting the latter – in addition to the 3-D ocean state itself – to further minimize the model-data misfit. By employing a strong constraint formulation of the assimilation algorithm, the final state estimate is dynamically and kinematically constrained, i.e. it satisfies the governing equations of continuity, momentum, temperature and salt conservation and the confines that bathymetry and coastline exert on the circulation.

A key motivation for this study was to compute a regional MDT that improved upon standard global products used in the satellite altimeter community. This is to enable calculation of absolute sea level above datum as the sum of MDT and satellite observed sea level anomaly with respect to a mean sea surface (the MSS having been removed to circumvent uncertainties in the marine geoid at short length scales). Our MDT from the mean of the ROMS TSV experiment successfully remedies several conspicuous shortcomings in AVISO MDT, and in so doing exhibits features of the mean sea level that are required for consistency with well-known observed aspects of the regional circulation. Notably, contours of constant MDT shoreward of the shelf break now closely parallel isobaths, recognizing that bathymetry strongly steers the depth-integrated currents. An along-shelf sea level slope of approximately 0.5×10^{-7} is a ubiquitous feature of mid-shelf waters, in agreement with previous 2-D idealized studies that note this term is significant in the along-shelf momentum balance.

On the northern outer shelf the sea level slope is moderately steeper, but in the southern MAB it reverses sign altogether, which contributes to driving across-isobath flow that partially drains the southwestward mean flow on the shelf. Despite this adverse pressure gradient, the along-shelf current steadily accelerates toward the south driving increasing offshore transport in the bottom Ekman layer. Nevertheless, the majority of along-shelf transport still remains on the shelf, continuing southward until it makes an abrupt turn seaward immediately north of Cape Hatteras.

The analysis has thus added quantitative, 3-dimensional detail to our view of the mean circulation in the MAB that was previously based principally on 2-D idealized or spatially localized studies, or on forward modeling studies that were largely unconstrained by historical observations.

The analyzed MDT from the ROMS TSV experiment is now being used in conjunction with coastal altimeter data to routinely assimilate those observations in the ESPreSSO near-real forecast system operated by MARACOOS. The MDT, 3-D velocity analysis, and MOCHA hydrographic atlas are also being used as a dynamically self-consistent ocean state climatology to adjust biases in sea level, velocity, temperature and salinity from global operational modeling systems before they are used as open boundary conditions data to the regional forecast system.

Acknowledgments

This work was supported by the NASA Ocean Surface Topography Science Team and NOAA Integrated Ocean Observing System. N. Fleming was supported by a Graduate Assistantship from Rutgers University. We are grateful to S. Lentz for making available his aggregation of historical long-term current meter deployment data, to C. Flagg for the *Oleander* ADCP data, and to the numerous researchers who have deposited their data in openly accessible and discoverable oceanographic data base systems maintained by IOOS partners and the U.S. National Centers for Environmental Information.

Supplementary materials

Supplementary material associated with this article can be found, in the online version, at doi:10.1016/j.ocemod.2018.05.003.

References

Beardsley, R.C., Boicourt, W.C., 1981. On estuarine and continental shelf circulation in the Middle Atlantic Bight. In: Warren, B.A., Wunsch, C. (Eds.), Evolution of Physical Oceanography. The MIT Press, Cambridge, MA, pp. 198–223.
Bennett, A.F., 2002. Inverse Modeling of the Ocean and Atmosphere. Cambridge University Press.
Boyer, T.P., Antonov, J.I., Baranova, O.K., Garcia, H.E., Johnson, D.R., Locarnini, R.A., Mishonov, A.V., O'Brien, T.D., Seidov, D., Smolyar, I.V., Zweng, M.M., 2009. World Ocean Database 2009. In: Levitus, S. (Ed.), NOAA Atlas NESDIS 66. U.S. Government Printing Office, Washington, D.C., pp. 216 DVDs.
Chassignet, E., Hurlburt, H.E., Metzger, E.J., Smedstad, O.M., Cummings, J., Halliwell, G.R., Bleck, R., Baraille, R., Wallcraft, A.J., Lozano, C., Tolman, H.L., Srinivasan, A., Hankin, S., Cornillon, P., Weisberg, R., Barth, A., He, R., Werner, F., Wilkin, J., 2009. U.S. GODAE: global ocean prediction with the HYbrid coordinate ocean model (HYCOM). Oceanography 22, 64–75.
Chassignet, E., Xu, X., 2017. Impact of horizontal resolution (1/12° to 1/50°) on Gulf Stream separation, penetration, and variability. J. Phys. Oceanogr. 47, 1999–2021.
Cipollini, P., Benveniste, J., Birol, F., Fernandes, J., Obligis, E., Passaro, M., Strub, P.T., Valladeau, G., Vignudelli, S., Wilkin, J., 2017. Satellite altimetry in coastal regions. In: Stammer, D., Cazenave, A. (Eds.), Satellite Altimetry Over Oceans and Land Surfaces. CRC Press, Boca Raton, pp. 343–380.
Cummings, J., 2005. Operational multivariate ocean data assimilation. Q. J. Royal Meteorol. Soc. 131, 3583–3604.
Dalyander, P.S., Butman, B., Sherwood, C.R., Signell, R.P., Wilkin, J., 2013. Characterizing wave- and current-induced bottom shear stress: U.S. Middle Atlantic

continental shelf. Cont. Shelf Res. 52, 73–86.
Dobricic, S., 2005. New mean dynamic topography of the Mediterranean calculated from assimilation system diagnostics. Geophys. Res. Lett. 32, L11606.
Feng, H., Vandemark, D., 2011. Altimeter data evaluation in the coastal Gulf of Maine and Mid-Atlantic Bight regions. Mar. Geodesy 34, 340–363.
Flagg, C., Dunn, M., Wang, D.-P., Rossby, H., Benway, R.L., 2006. A study of the currents of the outer shelf and upper slope from a decade of shipboard ADCP observations in the Middle Atlantic Bight. J. Geophys. Res. 111, C06003.
Fleming, N.E., 2016. Seasonal and spatial variability in temperature, salinity and circulation of the Middle Atlantic Bight (Ph.D. thesis). Rutgers University, New Brunswick, NJ, pp. 336. https://doi.org/http://dx.doi.org/10.7282/T3XW4N4M.
Gong, D., Kohut, J., Glenn, S., 2010. Seasonal climatology of wind-driven circulation on the New Jersey Shelf. J. Geophys. Res. 115, C04006.
Houghton, R., Schlitz, R., Beardsley, R., Butman, B., Chamberlin, J., 1982. The Middle Atlantic Bight cold pool: evolution of the temperature structure during summer 1979. J. Phys. Oceanogr. 12, 1019–1029.
Hu, J., Fennel, K., Mattern, J., Wilkin, J., 2012. Data assimilation with a local Ensemble Kalman Filter applied to a three-dimensional biological model of the Middle Atlantic Bight. J. Mar. Syst. 94, 145–156.
Lentz, S., 2008a. Observations and a model of the mean circulation over the Middle Atlantic Bight continental shelf. J. Phys. Oceanogr. 38, 1203–1221.
Lentz, S., 2008b. Seasonal variations in the circulation over the Middle Atlantic Bight continental shelf. J. Phys. Oceanogr. 38, 1486–1500.
Lin, Y.-T., Newhall, A., Potty, G.R., Miller, J.H., 2017. A preliminary numerical model of three-dimensional underwater sound propagation in the Block Island Wind Farm area. J. Acoust. Soc. Am. 141, 3933.
Linder, C., Gawarkiewicz, G., 1998. A climatology of the shelfbreak front in the Middle Atlantic Bight. J. Geophys. Res. 103 (18), 405–418 423.
Mannino, A., Signorini, S., Novak, M., Wilkin, J., Friedrichs, M., Najjar, R., 2016. Dissolved organic carbon fluxes in the Middle Atlantic Bight: an integrated approach based on satellite data and ocean model products. J. Geophys. Res. Biogeosci. 121, 312–336.
Maximenko, N., Niiler, P., Centurioni, L., Rio, M., Melnichenko, O., Chambers, D., Zlotnicki, V., Galperin, B., 2009. Mean dynamic topography of the ocean derived from satellite and drifting buoy data using three different techniques. J. Atmos. Ocean. Technol. 26, 1910–1919.
Mazloff, M.R., Gille, S.T., Cornuelle, B.D., 2014. Improving the geoid: combining altimetry and mean dynamic topography in the California coastal ocean. Geophys. Res. Lett. 41, 8944–8952.
Mesinger, F., DiMego, G., Kalnay, E., Mitchell, K., Shafran, P.E., W, Jovic, D., Woollen, J., Rogers, E., Berbery, E.E., M, Fan, Y., Grumbine, R., Higgins, W., Li, H., Lin, Y., Manikin, G., Parrish, D., Shi, W., 2006. North American regional reanalysis. Bull. Am. Meteorol. Soc. 87, 343–360.
Miles, T., Seroka, G., Glenn, S., 2017. Coastal ocean circulation during Hurricane Sandy. J. Geophys. Res. 122, 7095–7114.
Miles, T., Seroka, G., Kohut, J., Schofield, O., Glenn, S., 2015. Glider observations and modeling of sediment transport in Hurricane Sandy. J. Geophys. Res. 120, 1771–1791.
Moore, A.M., Arango, H., Broquet, G., Powell, B., Weaver, A.T., Zavala-Garay, J., 2011. The Regional Ocean Modeling System (ROMS) 4-dimensional variational data assimilations systems, Part I - System overview and formulation. Progress in Oceanography 91, 34–49.
Moore, A.M., Edwards, C., Fietcher, J., Drake, P., Neveu, E., Arango, H., Gurol, S., Weaver, A.T., 2013. A 4D-Var analysis system for the California Current: a prototype for an operational regional ocean data assimilation system. In: Xu, S.K.P.a.L. (Ed.), Data Assimilation for Atmospheric, Oceanic and Hydrologic Applications II. Springer, Berlin Heidelberg, pp. 345–365.
Pinardi, N., Allen, I., Demirov, E., De Mey, P., Korres, G., Lascaratos, A., Le Traon, P., Maillard, C., Manzella, G., Tziavos, C., 2003. The Mediterranean ocean forecasting system: first phase of implementation. Ann. Geophys. European Geosciences Union 21, 3–20.
Ridgway, K.R., Dunn, J.R., Wilkin, J.L., 2002. Ocean interpolation by 4-dimensional weighted least squares: application to the waters around Australasia. J. Atmos. Oceanic Technol. 19, 1357–1375.
Rio, M.-H., Guinehut, S., Larnicol, G., 2011. New CNES-CLS09 global mean dynamic topography computed from the combination of GRACE data, altimetry, and in situ measurements. J. Geophys. Res. 116, C7.
Rio, M.-H., Mulet, S., Picot, N., 2014a. Beyond GOCE for the ocean circulation estimate: synergetic use of altimetry, gravimetry, and in situ data provides new insight into geostrophic and Ekman currents. Geophys. Res. Lett. 41, 8918–8925.
Rio, M.-H., Pascual, A., Poulain, P., Menna, M., Barceló, B., Tintoré, J., 2014b. Computation of a new mean dynamic topography for the Mediterranean Sea from model outputs, altimeter measurements and oceanographic in situ data. Ocean Sci. 10, 731–744.
Roarty, H., Glenn, S., Kohut, J., Gong, D., Handel, E., Rivera Lemus, E., Garner, T., Atkinson, L., Jakubiak, C., Brown, W., Muglia, M., Haines, S., Seim, H., 2010. Operation and application of a regional high frequency radar network in the Mid Atlantic Bight. Mar. Technol. Soc. J. 44, 133–145.
Rossby, T., Gottlieb, E., 1998. The Oleander project: monitoring the variability of the Gulf Stream and adjacent waters between New Jersey and Bermuda. Bull. Am. Meteorol. Soc. 79, 5–18.
Sasaki, Y., 1970. Some basic formulations in numerical variational analysis. Mon. Weather Rev. 98, 875–883.
Seroka, G., Miles, T., Xu, Y., Kohut, J., Schofield, O., Glenn, S., 2017. Rapid shelf-wide cooling response of a stratified coastal ocean to hurricanes. J. Geophys. Res. 122, 4845–4867.
Shchepetkin, A.F., McWilliams, J.C., 2009. Computational kernel algorithms for fine-scale, multiprocess, longtime oceanic simulations. Handbook of Numerical Analysis. Comput. Methods Atmos. Oceans 14, 121–183.
Toole, J., Curry, R.G., Joyce, T., McCartney, M., Pena-Molino, B., 2011. Transport of the North Atlantic Deep Western Boundary Current about 35 N, 70W: 2004-2008. Deep Sea Research II 58, 1768–1780.
Ullman, D., O'Donnell, J., Kohut, J., Fake, T., Allen, A., 2006. Trajectory prediction using HF radar surface currents: Monte Carlo simulations of prediction uncertainties. J. Geophys. Res. 111, C12005. https://doi.org/10.1029/2006JC003715.
Vignudelli, S., Kostianoy, A., Cipollini, P., Benveniste, J., 2011. Coastal Altimetry. Springer, Berlin.
Warner, J., Sherwood, C., Arango, H., Signell, R., 2005. Performance of four turbulence closure models implemented using a generic length scale method. Ocean Model. 8, 81–113.
Weaver, A., Vialard, J., Anderson, D., 2003. Three-and four-dimensional variational assimilation with a general circulation model of the tropical Pacific Ocean. Part I: formulation, internal diagnostics, and consistency checks. Month. Weather Rev. 131, 1360–1378.
Wilkin, J., Hunter, E., 2013. An assessment of the skill of real-time models of Mid-Atlantic Bight continental shelf circulation. J. Geophys. Res. 118, 2919–2933. https://doi.org/10.1002/jgrc.20223.
Xu, Y., Cahill, B., Wilkin, J., Schofield, O., 2013. Role of wind in regulating phytoplankton blooms on the Mid-Atlantic Bight. Cont. Shelf Res. 63, S26–S35.
Zavala-Garay, J., Wilkin, J., Levin, J., 2014. Data assimilation in coastal oceanography: IS4DVAR in the Regional Ocean Modeling System (ROMS). In: Blayo, E., Bocquet, M., Cosme, E., Cugliandolo, L. (Eds.), Advanced Data Assimilation For Geosciences: Lecture Notes of the Les Houches School of Physics. Oxford University Press, Oxford, pp. 555–576 Special issue June 2012.
Zhang, W., Gawarkiewicz, G., McGillicuddy Jr, D., Wilkin, J., 2011. Climatological mean circulation at the New England shelf break. J. Phys. Oceanogr. 41, 1874–1893.